Semiconductor Physics, Quantum Electronics & Optoelectronics, 2007. V. 10, N 4. P.1-8.

PACS 85.40.Ls

Development of high-stable contact systems to gallium nitride microwave diodes

A.E. Belyaev[1], N.S. Boltovets[2], V.N. Ivanov[2], L.M. Kapitanchuk[3], V.P. Kladko[1], R.V. Konakova[1], Ya.Ya. Kudryk[1], A.V. Kuchuk[1], O.S. Lytvyn[1], V.V. Milenin[1], V.N. Sheremet[1], Yu.N. Sveshnikov[4]

[1]V. Lashkaryov Institute of Semiconductor Physics, NAS of Ukraine
41, prospect Nauky, 03028 Kyiv, Ukraine
Phone: +(380-44) 525-61-82; fax: +(380-44) 525-83-42; e-mail: konakova@isp.kiev.ua
[2]State Enterprise Research Institute "Orion", 8a, Eugene Pottier Str., 03057 Kyiv, Ukraine
Phone: +(380-44) 456-05-48; e-mail: bms@i.kiev.ua
[3]E.O. Paton Electric Welding Institute, NAS of Ukraine, Kyiv, Ukraine
[4]Close Corporation "Elma-Malakhit", Zelenograd, Russia; e-mail: info@emal.zelcom.ru

Abstract. High-stable heat-resistant low-resistance contact systems with diffusion barriers involving quasi-amorphous TiB_x layers are suggested and studied. We have performed the structural and morphological investigations along with studies of Auger concentration depth profiles in the contacts both before and after rapid thermal annealing. It is found that the Au–TiB_x–Al–Ti–GaN contact layers with diffusion barriers retain both a layered structure of the contact metallization and the value of contact resistivity practically unchanged up to the temperature $T \approx 700$ ºC. At the same time, the layered structure of the metallization in standard Au–Ti–Al–Ti–GaN contact systems breaks down at such rapid thermal annealing. It is shown that the contact metallization of both types demonstrates the tunnel current flow mechanism in the temperature range 225–335 K, whereas the current flow mechanism is thermionic in the range 335–380 K, the Schottky barrier height being ~0.16 eV. For the best samples under consideration, the contact resistivity was no more than 10^{-6} Ohm·cm^2.

Keywords: gallium nitride, ohmic contact, tunnel current, dislocation density, diffusion barrier.

Manuscript received 03.09.07; accepted for publication 00.00.07; published online 00.00.07.

1. Introduction

The wide-gap semiconductor gallium nitride has been used in optoelectronics for many years. Due to novel high-tech advances, it became practicably possible to develop microwave diodes and transistors based on GaN and its solid solutions [1-3]. The interest in such microwave devices is generated, first of all, by extension of the operating temperature range (up to 800 °C). In this case, along with requirements for high heat resistance of the main material (GaN), even the heavier demands are imposed on the barrier-forming and ohmic contacts. That is why the search for appropriate materials for contact systems is still in progress [2-8].

Earlier, we have studied the barrier and ohmic contacts based on amorphous interstitial phases (TiB_x, ZrB_x, NbN_x, TiN_x) to Si, GaAs, InP, and SiC microwave diodes. In those contacts, there were practically no interactions between phases up to temperatures over twice the operating ones [7, 9, 10]. Here, we apply the experience gained to the formation of ohmic contacts to *n*-GaN epitaxial layers grown on sapphire α-Al_2O_3.

2. Samples and investigation techniques

The n_1^+-n-n^+-GaN-i-Al_2O_3 epitaxial structures to be studied were MOVPE-grown at the Closed Corporation "Elma-Malakhit" (Zelenograd, Russia). The concentration of donor impurity (silicon) in the *n*-region was $(1–2)\times10^{17}$ cm^{-3}, while that in the n^+-region did not exceed 6×10^{18} cm^{-3}. The thicknesses of the *n*- and n^+-layers were ~1.5–2 and ~0.8–1 μm, respectively.

The structural perfection of two GaN epitaxial structures (#1 and #2) was studied using high-resolution

© 2007, V. Lashkaryov Institute of Semiconductor Physics, National Academy of Sciences of Ukraine

x-ray diffraction (XRD). The measurements were made with a diffractometer "PANalytical X'Pert MRD". We used a measuring circuit with an analyzer before a detector. This makes it possible to obtain two sections of the reciprocal lattice sites, namely, those perpendicular and parallel to the diffraction vector – ω-scan and ω–2θ-scan, respectively. We measured the half-widths of those sections for the symmetric reflections, 0002 and 0004, and asymmetric reflections, $1\bar{1}04$ and $11\bar{2}4$, in two directions about the diffraction vector **H** (Table 1).

Strain is not the only reason for the broadening of reflection peaks. Another factor affecting the sites shape lies in the limited sizes of coherent-scattering regions [11]. The contributions from the two factors can be discriminated in XRD measurements. One should proceed from the considerations that the distortion components make broader only the reflections having the corresponding components of the diffraction vector, $\delta q_i = \langle \delta e_{ji} \rangle H_j$, while the limitation of the sizes of coherent-scattering regions affects all reciprocal lattice sites along the diffraction vector.

The relation between coordinates in the reciprocal space and the angular broadening of XRD curves depends on the scan mode, i.e., the scan direction relative to the diffraction vector [12]. For the scan section along the diffraction vector, $\delta w = \delta q_{\mathrm{H}} / k \cos \vartheta_{\mathrm{B}}$, while $\delta w = \delta q_{\perp} / \mathrm{H}$ in the perpendicular direction.

An example of the distribution of symmetric Bragg reflection intensity around the reciprocal lattice site 0002 is given in Fig. 1. The intensity contours are extended along the normal to the diffraction vector **H**, and their form is typical of relaxed structures. Such a form of the intensity contours around the reciprocal lattice sites is characteristic of structure #1.

The extension of the diffraction intensity distribution around the reciprocal lattice sites in parallel to the sample surface is related to the anisotropy of the fields of elastic stresses in the layers. For structure #2, the contours shape is practically symmetric for two directions about the diffraction vector.

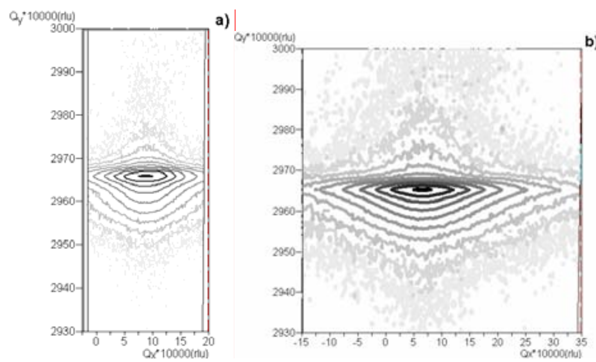

Fig. 1. Two-dimensional maps of XRD curve intensity distribution around the reciprocal lattice site 0002 for two GaN/Al_2O_3 epitaxial structures.

Table 1. Half-widths (in the seconds of arc) of diffraction reflection curves and their ratios in GaN samples.

GaN sample #	ω 0002	ω–2θ 0002	ω 0004	ω–2θ 0004	$11\bar{2}4/11\overline{24}$
1	210	46	187	81	127/356
2	88	49	62	61	283/375

Table 2. Distortion tensor components (δe_{zz}, δe_{zx}, δe_{xz}, and δe_{xx}), sizes of coherent-scattering regions (τ_z and τ_x), and dislocation density ρ in GaN layers.

GaN sample #	$10^4\delta e_{zz}$	$10^4\delta e_{zx}$	$10^4\delta e_{xz}$	$10^4\delta e_{xx}$	τ_z, nm	τ_x, nm	$10^{-8}\rho$, cm^{-2}
1	2.57	9.3	6.1	3.92	480	80	1.38
2	2.67	7.1	6.3	2.9	525	160	1.08

The tangential character of the ω–2ϑ-curves in higher-order reflections suggests that the main contribution to broadening comes from strains [13]. The characteristic feature of the films is that, in asymmetric geometry $11\bar{2}4$, the half-widths of reflection curves at the grazing incidence were considerably below than those at the glancing reflection (see the last column in Table 1). Such a behavior is characteristic of the case of reciprocal lattice site extension in parallel to the sample surface. For this reflection, the parallel and normal to **H** components of the diffraction vector are nearly the same, so the above situation can be attributed to the anisotropy of either the distortion components ($\delta e_{zx} > \delta e_{xz}$) or the shapes of coherent-scattering regions. According to the above interrelation, the extension of film #1 is much over that of film #2; the ratios between the curve half-widths being 0.35 and 0.75, respectively.

The values of strain tensor components were determined directly from the half-widths of reflection curves in the Bragg and Laue geometries (Table 2). One can see from Table 2 that the dilatation component of the microstrain tensor, δe_{xx}, is much over δe_{zz}. This suggests that the local variations of the interplanar spacing for the planes normal to the surface are much over those for the planes parallel to the interface. The interrelation between the off-diagonal components, $\delta e_{zx} > \delta e_{xz}$ (particularly for sample #1), shows that the disorientation of the planes parallel to the surface is bigger than that for the planes normal to the surface.

As to the densities of edge and screw dislocations, they are approximately the same. The estimated dislocation densities for the two samples under investigation are given in Table 2; the ratio between them is about one and a half. The sizes of grains (coherent-scattering regions) along the normal to the surface are much over the transverse ones.

The manufacturing scheme for chips with ohmic contacts (Fig. 2) is realized as follows. A nickel layer (~0.5 μm in thickness) is sputtered onto the starting n_1^+-n-n_2^+-GaN-i-Al_2O_3 structure using the electron-beam

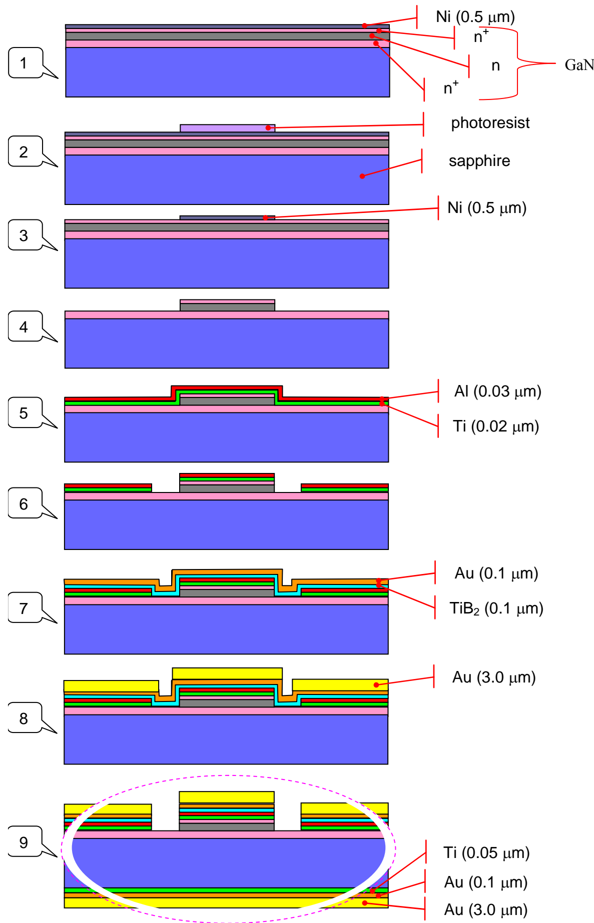

Fig. 2. Manufacturing scheme for ohmic contacts and Gunn diode chips based on n^+-n-n^+-GaN structures on sapphire.

evaporation technique (position 1 in Fig. 2). After this, a nickel mask is formed using photolithography (2) and chemical etching (3). Then the n^+- and n-layers are removed with ion-plasma etching (4), and the Ti and Al layers are deposited sequentially onto the structure obtained (5). After this, the contacts are separated using photolithography and etching of metallized structures down to the n_2^+-GaN layer (6). To form an ohmic contact, the Ti–Al layers are annealed for 30 s in the nitrogen atmosphere at a temperature of ~900 ºC. Then a TiB_x (or Ti) buffer layer is sputtered onto the ohmic contact structure obtained; after this, an Au layer is sputtered (7), and a rather thick (~3 μm) Au contact layer is formed by electrochemical deposition on the structure obtained (except the grooves) (8). The latter layer serves as a mask when chemically etching the TiB_x (Ti) and thin (~0.1 μm) sputtered gold layers (9). The diameter of the mesas obtained is determined by that of the nickel mask.

The contact resistivity was measured using a version of the radial geometry of contact pads applied in the transmission line method (TLM) [14]. To determine

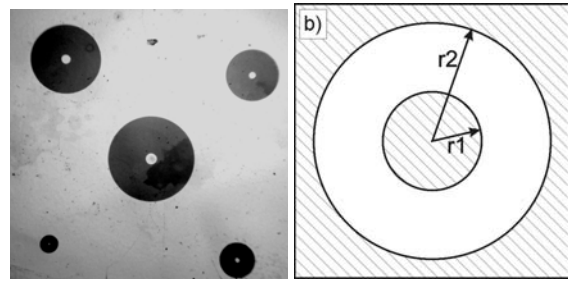

Fig. 3. Piece of a wafer with formed contacts for contact resistivity TLM measurements.

the ohmic contact resistivity in such a geometry, we used a mask (its fragment is shown in Fig. 3). It involves concentric contact pads (radii r_1 and r_2 are shown in Fig. 3). A single array had several such contact pads with different radii r_1 and r_2, for which the following requirement has to be met: $\ln\left(r_2/r_1\right) = C = \text{const}$. In this case, the resistance between the contact pads can be calculated within the TLM models from the expression

$$R_t = \frac{CR_s}{2\pi} + \frac{R_S}{2\pi}\frac{1}{\alpha r_1}\frac{I_0(\alpha r_1)}{I_1(\alpha r_1)}.$$

Here, R_t is the total resistance measured between the contact pads; R_s the semiconductor layer resistivity; $I_0(\alpha r_1)$ and $I_1(\alpha r_1)$ the zeroth- and first-order modified Bessel functions, respectively; $\alpha = \left(R_s/\rho_c\right)^{\frac{1}{2}}$; and ρ_c the ohmic contact resistivity.

Both before and after the rapid thermal annealing (RTA), we investigated the I–V curves of the Au–TiB_x (Ti)–Al–Ti–GaN contacts, contact resistivity ρ_c, concentration depth profiles of the contact components (Auger electron spectroscopy), GaN surface morphology after the removal of metallization (atomic force microscopy), and the XRD patterns of the Al–Ti–GaN and Au–TiB_x–Al–Ti–GaN contacts, as well as the temperature dependence of ρ_c for the Au–TiB_x–Al–Ti–GaN ohmic contacts.

3. Results and discussion

*A. Components distribution in the contacts***.** In Figs. 4 and 5, we show the Auger concentration depth profiles of (i) the Au–TiB_x (Ti)–Al–Ti–GaN contact components (taken before and after RTA at the temperature T = = 700 ºC), and (ii) the Au–TiB_x–Al–Ti–GaN contact components (taken before and after RTA at T = 900 ºC). These profiles characterize the processes of solid-state interactions at the metal–metal and metal–semiconductor interfaces.

According to the results obtained in [2, 4, 7], one may suppose that the following reactions can occur in both the above-mentioned contact systems as a result of RTA at T = 700 °C:

© 2007, V. Lashkaryov Institute of Semiconductor Physics, National Academy of Sciences of Ukraine

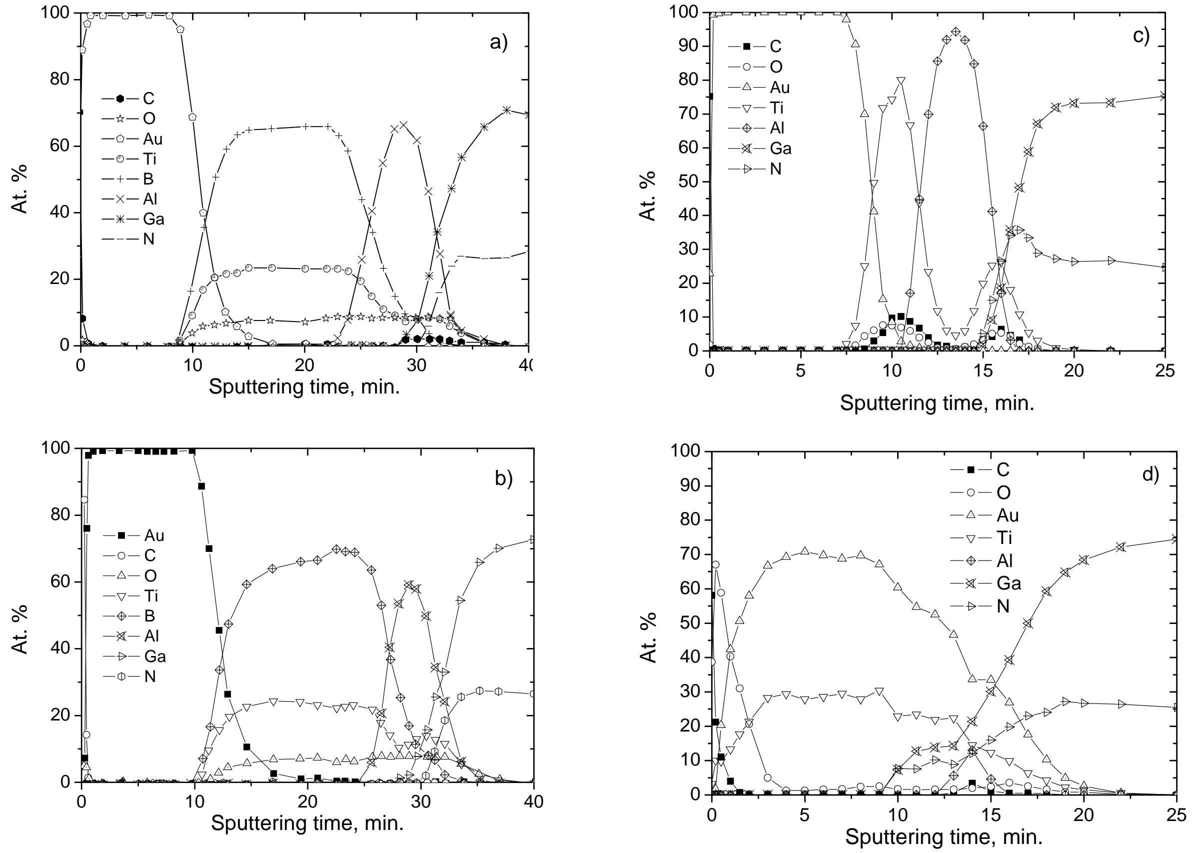

Fig. 4. Component concentration depth profiles in the contacts Au–TiB$_x$–Al–Ti–GaN (*a*, *b*) and Au–Ti–Al–Ti–GaN (*c*, *d*) before (*a*, *c*) and after RTA at T = 700 ºC (*b*, *d*).

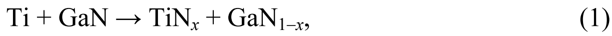

$$\mathrm{Ti} + \mathrm{GaN} \rightarrow \mathrm{TiN}_x + \mathrm{GaN}_{1-x}, \quad (1)$$

$$\mathrm{Ti} + 3\mathrm{Al} \rightarrow \mathrm{Al_3Ti}, \quad (2)$$

$$3\mathrm{Ti} + \mathrm{Al} \rightarrow \mathrm{AlTi_3} \quad (3)$$

This can lead to chemical nonuniformities at the interfaces and, as a result, increase their structural nonuniformity. The increase of the RTA temperature up to 900 °C for the Au–TiB$_x$–Al–Ti–GaN contact system leads to smearing out the contact layer structure (Figs. 4 and 5) and the enhancement of interactions between phases. One can see from the results presented in Figs. 4 and 5 that, if TiB$_x$ is replaced by Ti, the contact layer structure is damaged even by RTA at 700 °C.

The above results, however, indicate the presence of more complicated interaction processes occurring at the interfaces than those following from Eqs. (1)–(3). Oxygen takes an active part in those processes leading to the formation of oxynitride (oxyboride) phases. This, in turn, increases the semiconductor surface roughness.

B. Studies of the GaN surface morphology after the removal of metallization. The results of investigations with Auger electron spectroscopy agree with the data on the GaN surface morphology obtained with atomic force microscopy (after the removal of metallized layers) before and after RTA at T = 700 °C. The results of our studies of the surface morphology are presented in Fig. 6 and Table 3. It follows from them that the parameters of GaN surface roughness after the removal of metallization differ from those for the initial surfaces. This distinction is particularly pronounced when comparing with the initial non-metallized GaN surface (Table 3, the first row). One can see that the size of rough areas grew considerably. The above feature is more pronounced in the Au–Ti–Al–Ti–GaN rather than Au–TiB$_x$–Al–Ti–GaN contacts.

Table 3. Effect of RTA on the morphology of metal-GaN interfaces.

Sample type	Z_{range}, nm	R_{RMS}, nm	R_a, nm
n-GaN-Al_2O_3, initial	25	1.4	1.1
Au–TiB_2–Al–Ti/GaN, initial	182.3	12.2	8.4
Au–TiB_2–Al–Ti/GaN, annealed	372.4	47.1	36.4
Au–Ti–Al–Ti/GaN, initial	208.8	18.4	14.3
Au–Ti–Al–Ti/GaN, annealed	387.2	44.8	34.6

Z_{range} – difference between the highest and lowest surface points; R_{RMS} – root-mean-square roughness; R_a – arithmetic mean roughness.

© 2007, V. Lashkaryov Institute of Semiconductor Physics, National Academy of Sciences of Ukraine

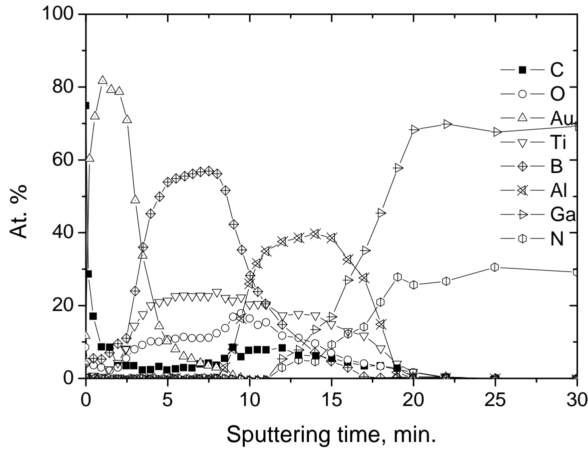

Fig. 5. Component concentration depth profiles in the Au–TiB_x–Al–Ti–GaN contacts after RTA at T = 900 ºC.

RTA leads to an increase of the roughness degree; this nonuniformity is more pronounced in the contacts with TiB_x layers. This fact can be due to the intense diffusion (mass transport) between phases or the formation and growth of new phases (e.g., ternary ones) at the metal–GaN interface, as it was observed for the Al–Ti–GaN ohmic contacts in [15].

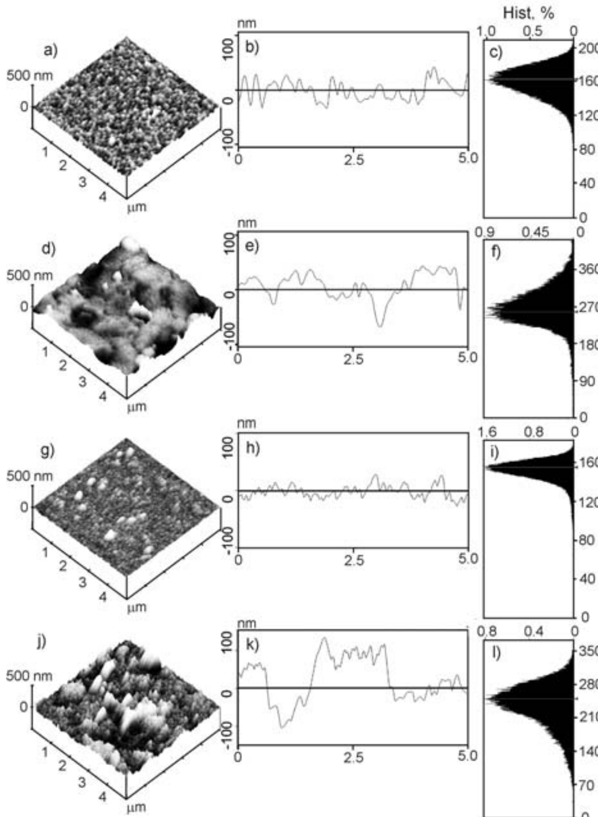

Fig. 6. GaN surface morphology (*a*, *d*, *g*, *j*), surface roughness (*b*, *e*, *h*, *k*), and histograms of roughness heights (*c*, *f*, *i*, *l*) after the removal of Au–Ti–Al–Ti (a-f) and Au–TiB_2–Al–Ti (*g-i*) metallizations before (*a-c*, *g*, *h*, *i*) and after RTA at T = 700 ºC (*d-f*, *j-l*).

C. x-ray phase analysis of contact metallization. We studied the contact phase composition to determine the predominant processes of phase formation in the contact metallization layers. The most intense interactions between phases were observed in the Au–TiB_x–Al–Ti–GaN contacts at the metal–semiconductor interface. That is why we chose them to perform x-ray phase analysis (XPA) in the following sequence:

- XPA of the starting (before RTA) Al–Ti–GaN-*i*-Al_2O_3 contacts;
- XPA of the Al–Ti–GaN-*i*-Al_2O_3 contacts after RTA at T = 700 °C;
- XPA of the Al–TiB_x–Al–Ti–*n*-GaN-*i*-Al_2O_3 contacts.

One can see from the XPA results given in Fig. 7 that reflection (0002) from the GaN epitaxial layer is present in the XRD patterns of both the initial Al–Ti–GaN-*i*-Al_2O_3 structure and that after RTA. In addition, reflection (0006) from the Al_2O_3 substrate is observed in the XRD pattern of the initial structure. Strong disorientation of both the substrate and the epitaxial layer is the reason for the absence of the above reflection in the XRD patterns taken after RTA. In addition, the reflections from Al, Ti, and Al_2Ti are observed in the initial sample. The Al_2Ti phase seems to be formed in the course of magnetron sputtering of the metal.

No reflections from Ti were detected in the Al–Ti–GaN-*i*-Al_2O_3 contacts after RTA, while those from Ti_2AlN, Al_3Ti and $AlTi_3$ were observed. We assume that, due to high-temperature conditions, the Al atoms penetrate through the Ti film and form the ternary phase Ti_2AlN at the Ti–GaN interface. The presence of reflections from Al after RTA shows that the Al-involved reaction was incomplete. Sputtering the Au–TiB_x layers onto the Al–Ti–GaN-*i*-Al_2O_3 structure after RTA does not change considerably the phase composition of metallization. In this case, the additional reflections (those from Au) were detected in the XRD pattern. TiB_x was in a quasi-amorphous phase.

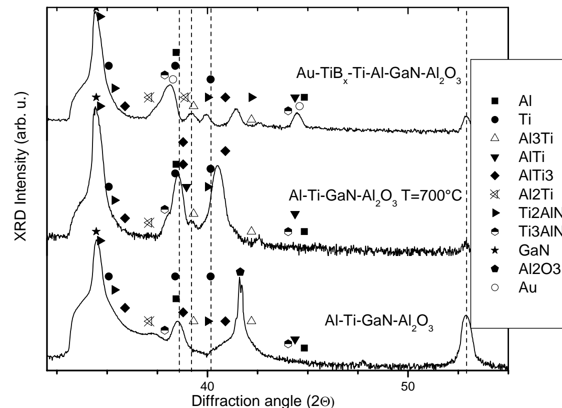

Fig. 7. XRD patterns of the Al–Ti–GaN-*i*-Al_2O_3 structure before (*1*) and after RTA at 700 ºC (*2*) and Au–TiB_x–Al–Ti–GaN-*i*-Al_2O_3 after RTA at 900 ºC (*3*).

© 2007, V. Lashkaryov Institute of Semiconductor Physics, National Academy of Sciences of Ukraine

No reflections from TiN_x were detected in the XRD patterns presented in Fig. 7. The reason for this seems to be either the temperature insufficiently high to form the TiN_x phase or the too small duration of thermal annealing. At the same time, it was shown in our work [10] with XPA that the increase of the RTA temperature up to 870 °C leads to the formation of TiN_x in such contacts, and this results in the decrease in ρ_c down to $\sim 10^{-6}$ Ohm·cm^2. However, this is not at variance with the above results that correlate with the data obtained using Auger electron spectroscopy and atomic force microscopy.

D. I–V curves. In Fig. 8, we present the *I–V* curves for Au–TiB_x–Al–Ti–n^+-n-n^+-GaN contacts taken in the temperature range 90–380 K. They demonstrate a good linearity over the whole temperature range. Such a feature can be explained by the fact that the current through the structure is determined by the semiconductor resistance. This can be seen from the comparison of the structure total resistance and the calculated contact resistance. Another evidence is the temperature dependence of the charge carrier mobility in our contacts (Fig. 9a, curve 5), which correlates well with the temperature dependence of electron mobility in GaN (Fig. 9a, curves 1-4) described in [16]. The conductivity peak position for our contact fits quite well the general dependence of the positions of charge carrier mobility peaks on the impurity concentration.

E. Temperature measurements of contact resistance. The results of measurements of the contact resistivity ρ_c in the temperature range 225–380 K show that the $\ln\rho_c = f(T)$ curve has two different sections of the variation of ρ_c (Fig. 10):

(i) in the temperature range 225–335 K, ρ_c practically does not depend on temperature; this indicates the tunnel mechanism of the current flow through the contact (Fig. 10a, section 1);

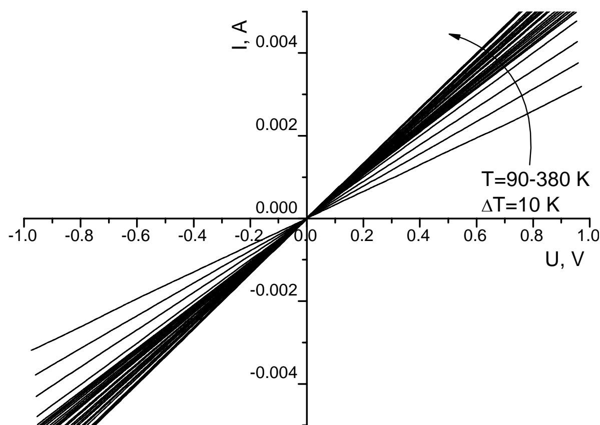

Fig. 8. *I–V* curves of the Au–TiB_x–Al–Ti–n^+-n-n^+-GaN contact in the temperature range 90–380 K.

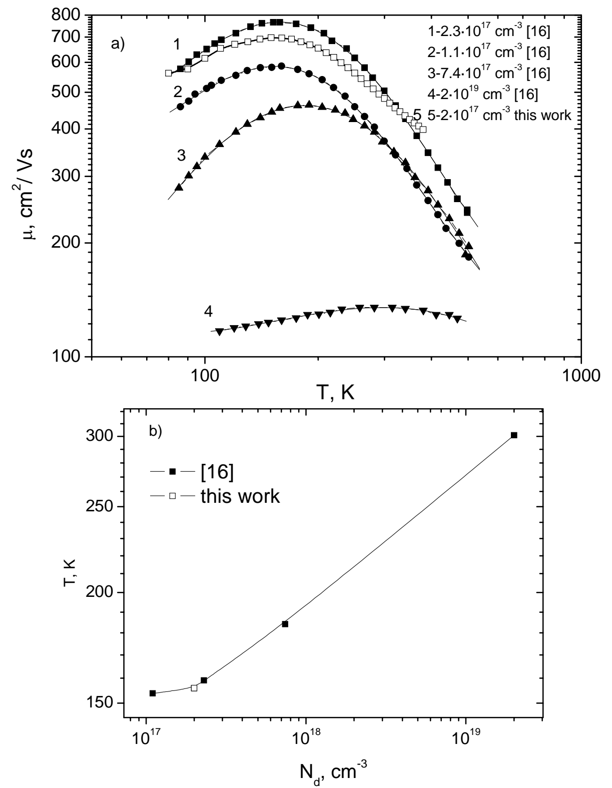

Fig. 9. (*a*) – temperature dependence of the charge carrier mobility at different impurity concentrations taken from [16] (curves *1-4*) in comparison with that in our contacts (curve *5*); (*b*) – dependence of the positions of peaks of the above curves on the noncompensated impurity concentration.

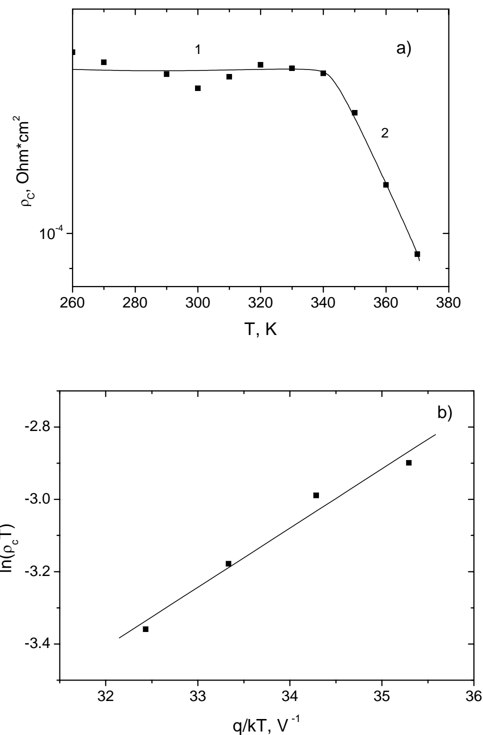

Fig. 10. Temperature dependence of the contact resistivity in semilogarithmic coordinates (*a*) and the $\ln(\rho_c T) = f(q / kT)$ curve (*b*).

© 2007, V. Lashkaryov Institute of Semiconductor Physics, National Academy of Sciences of Ukraine

(ii) in the temperature range 335–380 K, ρ_c decreases exponentially with temperature (Fig. 10a, section 2). The function ln ($\rho_c T$) = f(1/T) is linear in T (Fig. 10b); this indicates the thermionic mechanism of current flow (Fig. 9, section 2).

The Schottky barrier height φ_B was determined from the $\ln(\rho_c T) = f(q/kT)$ plot in the temperature range 335–380 K (Fig. 10b). We obtained $\varphi_B \approx 0.16$ eV.

As to the nature of the current through the contact in the temperature range 225–335 K, it seems to be determined by the tunnel current flow through dislocations. As was shown before, their density in our samples was ~10^8 cm^{-2}. The dislocation current flow mechanism in GaN Schottky barrier diodes was observed by us in [17]; in that case, the dislocation density in GaN was ~10^8–10^{10} cm^{-2}. A similar mechanism has been advanced earlier in [18] for the description of the temperature dependence of the saturation current in surface-barrier diodes based on GaAs and GaP. In that case, the dislocation density in the semiconductor near-contact region was sufficiently high (≥ 10^{-8} cm^{-2}) [18, 19].

Such current flow mechanism proved to be typical of the Au–TiB_x (Ti)–Al–Ti–n-GaN ohmic contacts studied by us. Both the current flow mechanism and the ohmic contact parameters were not changed considerably after the repeated RTA (T = 700 and 870 °C) of the Au–TiB_x–Al–Ti–n-GaN contacts. This indicates their thermal stability. At the same time, the repeated RTA (T = 700 °C) of the Au–Ti–Al–Ti–n-GaN contacts increased ρ_c by a factor of 2 – 3, the current flow mechanism in the temperature range 90–380 K remaining the same.

In the best samples of GaN epitaxial structures with ohmic contacts involving TiB_x layers as diffusion barriers, the contact resistivity was ~10^{-6} Ohm·cm^2. So they are suitable for the application when making microwave diodes (Schottky barrier and Gunn ones) [20].

8. Conclusion

We have shown that it is possible to form stable (up to $T \approx 700$ ºC) ohmic contacts to the GaN n^+-n-n^+ epitaxial structures, with a contact resistivity of ~10^{-6} Ohm·cm^2 (for the best samples), on the basis of the contact metallization with TiB_x buffer layers. The current flow in such contacts (in the temperature range 225–235 K) occurs by the tunneling of charge carriers in accordance with the dislocation mechanism. The dislocation density in the GaN epitaxial layers is ≥ 10^8 cm^{-2}; this is enough for charge carriers to tunnel through a barrier. In the temperature range 335–380 K, the thermionic current flow mechanism is observed, the height of the Schottky barrier in the contact being ~0.16 eV.

It is shown that RTA (T = 700 ºC) of the standard Au–Ti–Al–Ti–n-GaN ohmic contact leads to the mixing of metallization layers. This makes the degradation of such contacts easier.

The results obtained should be taken into account when developing a manufacturing technology for contacts to gallium nitride.

References

1. Yu.G. Shretter, Yu.T. Rebane, V.A. Zykov, V.G. Sidorov, *Wide-Gap Semiconductors.* Nauka, St.-Petersburg, 2001 (in Russian).
2. H. Morkoç, *Nitride Semiconductors and Devices*. Springer, Berlin, 1999.
3. V.N. Danilin, Yu.P. Dokuchaev, T.A. Zhukova, M.A. Komarov, High-power high-temperature capable and radiation-resistant microwave devices of new generation with wide-gap AlGaN/GaN heterojunction structures // *Obzory po Elektronnoi Tekhnike*, *Ser. 1. SVCh Tekhnika*. State Unitary Enterprise Research Institute “Pulsar”, Moscow, 2001 (in Russian).
4. P. Kordoš, GaN-based electronics: Material and device issues, in: *Proc. ASDAM-2000,* Smolenice Castle, Slovakia, 2000, p. 47-54.
5. M.S. Noor, Contact mechanisms and design principles for alloyed ohmic contacts // *J. Appl. Phys*. **95**(12), p. 7940-7953 (2004).
6. N.A. Papanicolaou, K. Zekentes, High temperature characteristics of Ti/Al and Cr/Al ohmic contacts to n-type GaN // *Solid-State Electron*. **46**, p. 1975-1981 (2002).
7. A.E. Belyaev, N.S. Boltovets, V.N. Ivanov, R.V. Konakova, Ya.Ya. Kudryk, P.M. Lytvyn, V.V. Milenin, Yu.N. Sveshnikov, Thermal stability of multilayer contacts formed on GaN // *Pis’ma v Zh. Tekh. Fiz.* **31**(24), p. 88-94 (2005) (in Russian); *Techn. Phys. Lett*. **31**(12), p. 1078 (2005).
8. F. Lucolano, F. Roccaforte, F. Giannazo, A. Alberti, V. Raineri, Current transport in Ti/Al/Ni/Au ohmic contacts to GaN and AlGaN // *Mater. Sci. Forum* **556-557**, p. 1027-1030 (2007).
9. N.S. Boltovets, V.N. Ivanov, R.V. Konakova, Ya.Ya. Kudryk, O.S. Lytvyn, P.M. Lytvyn, V.V. Milenin, Interactions between phases and the features of structural relaxation in TiB_x-n-GaAs (InP, GaP, 6H SiC) contacts exposed to active treatments // *Fizika Tekhnika Poluprovodnikov* **38**(7), p. 769-774 (2004) (in Russian).
10. A.E. Belyaev, N.S. Boltovets, V.N. Ivanov, V.P. Kladko, R.V. Konakova, A.V. Kuchuk, Ya.Ya. Kudryk, O.S. Lytvyn, V.V. Milenin, Yu.N. Sveshnikov, Heat-resistant Au-TiB_x-n-GaN Schottky diodes, in: *Proc. of the 16th Intern. Crimean Conf. “Microwave & Telecommunication Technology”,* September 11-15, 2006, Sevastopol, Weber, p. 644-645 (2006).
11. A.S. Usikov, V.V. Tretyakov, A.V. Bobyl, R.N. Kyutt, V.V. Lundin, B.V. Pushnyi, N.M. Shmidt, Internal microstresses, distribution of

© 2007, V. Lashkaryov Institute of Semiconductor Physics, National Academy of Sciences of Ukraine

composition and cathodoluminescence over section of $Al_xGa_{1-x}N$ epitaxial layers on sapphire // *Fizika Tekhnika Poluprovodnikov* **34**(11), p. 1300-1306 (2000) (in Russian).
12. V.P. Kladko, S.V. Chornen'kii, A.V. Naumov, A.V. Komarov, M. Tasapo, Yu.N. Sveshnikov, S.A. Vitusevich, A.E. Belyaev, Structural defects at heteroboundaries and photoluminescence properties of GaN and $Al_xGa_{1-x}N$/GaN epitaxial layers grown on sapphire // *Fizika Tekhnika Poluprovodnikov* **40**(9), p. 1087-1093 (2006) (in Russian); *Semiconductors* **40**, p.1060 (2006).
13. V.V. Ratnikov, R.N. Kyutt, T.V. Shubina, T. Paskova, B. Monemar, Determination of microdistortion components and their application to structural characterisation of HVPE GaN epitaxial layers // *J. Phys. D: Appl. Phys*. **34**, p. A30-A34 (2001).
14. A.N.Andreev, M.G. Rastegaeva, V.P. Rastegaev, S.A. Reshanov, On allowance for current spreading in a semiconductor when determining resistance of ohmic contacts // *Fizika Tekhnika Poluprovodnikov* **32**(8), p. 832-837 (1998) (in Russian).
15. Joon Scop Kwak, S.E. Mohney, Je-Yi Lin, R.S. Kern, Low resistance Al/Ti/*n*-GaN ohmic contacts with improved surface morphology and thermal stability // *Semicond. Sci. Technol*. **15**, p. 756-760 (2000).
16. W. Götz, N.M. Johnson, C. Chen, H. Lin, C. Kuo, W. Imler, Activation energies of Si donors in GaN // *Appl. Phys. Lett*. **68**(22), p. 3144-3146 (1996).
17. A.E. Belyaev, N.S. Boltovets, V.N. Ivanov, V.P. Kladko, R.V. Konakova, Ya.Ya. Kudryk, A.V. Kuchuk, V.V. Milenin, Yu.N. Sveshnikov, V.N. Sheremet, On the tunneling current flow mechanism in Au-TiB_x-*n*-GaN-*i*-Al_2O_3 Schottky barrier diodes // *Semiconductor Physics, Quantum Electronics and Optoelectronics* **10**(3), p. 1-5 (2007).
18. V.V. Evstropov, M. Dzhumaeva, Yu.V. Zhilyaev, N. Nazarov, A.A. Sitnikova, L.M. Fedorov, Dislocation nature and model for excess-tunneling current in the *p-n* structures on the basis of GaP // *Fizika Tekhnika Poluprovodnikov* **34**(11), p. 1357-1362 (2000) (in Russian); *Semiconductors* **34**, p. 1305 (2000).
19. V.V. Evstropov, Yu.V. Zhilyaev, M. Dzhumaeva, N. Nazarov, Tunnel-excess current in $A^{III}B^{V}$ nondegenerate barrier *p-n* and *m-s* structures on Si // *Fizika Tekhnika Poluprovodnikov* **31**(2), p. 152-158 (1997) (in Russian); *Semiconductors* **31**, p. 115 (1997).
20. M. Shur, *GaAs Devices and Circuits*. Plenum Press, New York–London, 1987.

© 2007, V. Lashkaryov Institute of Semiconductor Physics, National Academy of Sciences of Ukraine